Applied Catalysis B: Environmental 199 (2016) 439–446

Contents lists available at ScienceDirect

Applied Catalysis B: Environmental

journal homepage: www.elsevier.com/locate/apcatb

Base metal-Pt alloys: A general route to high selectivity and stability in the production of biofuels from HMF

Jing Luo[a], Jennifer D. Lee[b], Hongseok Yun[b], Cong Wang[a], Matteo Monai[c], Christopher B. Murray[b], Paolo Fornasiero[c], Raymond J. Gorte[a,*]

[a] Department of Chemical & Biomolecular Engineering, University of Pennsylvania, Philadelphia, PA 19104, United States
[b] Department of Chemistry, University of Pennsylvania, Philadelphia, PA 19104, United States
[c] Department of Chemical and Pharmaceutical Sciences, ICCOM-CNR and INSTM Trieste Research Unit, University of Trieste, Trieste, 34127, Italy

ARTICLE INFO

Article history:
Received 23 May 2016
Received in revised form 15 June 2016
Accepted 21 June 2016
Available online 22 June 2016

Keywords:
5-Hydroxymethylfurfural
Hydrodeoxygenation
2,5-Dimethyl furan
Nanocrystal
Bimetallic catalyst

ABSTRACT

Hydrodeoxygenation (HDO) of 5-hydroxymethylfurfural (HMF) was examined over well-defined and uniform, Pt-Ni, Pt-Zn and Pt-Cu alloyed nanocrystals (NCs) supported on carbon, at 33 bar and between 160 and 200 °C. Pt-Ni alloy catalysts were prepared in three different Pt:Ni ratios, Pt_6Ni, Pt_3Ni, and PtNi. While all of the Pt-Ni alloys were more selective for producing 2,5-dimethylfuran (DMF) than were Pt or Ni monometallic catalysts, the Pt_3Ni catalyst was superior to the other compositions, exhibiting a yield of 98% due to its optimum surface composition. Similarly high yields were obtained on catalysts prepared from Pt_2Zn and PtCu NCs. Possible reasons are given for why each of the Pt-alloy catalysts is highly selective.

1. Introduction

The conversion of biomass into fuels and other petrochemical replacements is receiving an ever increasing amount of attention as concerns about sustainability grow. Among the more important reactions for utilizing biomass is the hydrodeoxygenation (HDO) of 5-hydroxymethylfurfural (HMF) to 2,5-dimethylfuran (DMF). HMF is produced by the acid-catalyzed dehydration of C-6 sugars [1–3] but is too unstable to be used directly in most applications due to its high degree of chemical functionality. The conversion of HMF to DMF consumes relatively little hydrogen (HMF:H_2 molar ratio 1:3) and results in a product that can be used directly as a fuel additive. DMF can also be reacted with ethylene to produce *p*-xylene in high yields [4], demonstrating that an important chemical feedstock can be produced from renewable resources.

Achieving high selectivities (>90%) in the reaction of HMF to DMF remains a problem. Possibly because the reaction products depend strongly on reactor conditions, a wide range of selectivities have been reported by the various groups which have studied the problem [5–7], sometimes for similar catalysts. However, for monometallic catalysts, yields are generally below 60%. Work from our groups has shown that the HDO of HMF is a series reaction over most carbon-supported, monometallic catalysts, with DMF forming as an intermediate product that can further react [8]. On carbon-supported Pt, Pd, Ir, Ni, Ru, and Co catalysts, DMF is converted to the undesired ring-opened (e.g. 2-hexanone, 2,5-hexanedione) and ring-hydrogenated (e.g. 2,5-dimethyltetrahydrofuran, DMTHF) products under the conditions required to react HMF to DMF [8]. Because of this, the maximum yield of a given catalyst depends on the relative rates of HMF converting to DMF and of DMF converting to other products.

There is considerable evidence that bimetallic catalysts can be more selective for HDO reactions. For example, in the gas-phase reaction of furfural, Ni-Fe catalysts were found to exhibit good selectivity to methylfuran under conditions that resulted in the decarbonylation product, furan, over the monometallic Ni catalyst [9]. In another example involving the reaction of HMF, Wang et al. [10] reported that catalysts based on Pt-Co nanoparticles, encapsulated in hollow carbon spheres, could give DMF yields as high as 98%. We have recently confirmed this result on carbon-supported Pt-Co nanocrystals (NCs), without the carbon hollow-spheres, and further showed that the bimetallic catalysts exhibit much better stability than the monometallic catalysts [11]. The high selectivity

* Corresponding author at: Department of Chemical and Biomolecular Engineering, University of Pennsylvania, 311A Towne Building, 220 S. 33rd Street, Philadelphia, PA 19104, United States.
E-mail addresses: jingluo@seas.upenn.edu (J. Luo), joshua.zju@gmail.com, gorte@seas.upenn.edu (R.J. Gorte).

http://dx.doi.org/10.1016/j.apcatb.2016.06.051
0926-3373/

of the Pt-Co catalysts resulted from the fact that DMF is unreactive over the bimetallic catalyst.

It is not entirely clear why the bimetallic catalysts are more selective for HDO and the reasons may vary with the particular alloy or reactor conditions. Several studies have argued the high selectivities of the studied bimetallic catalysts is due to the oxophilicity of the secondary metal [9,12–14]. For example, Resasco and coworkers [9] observed that Ni-Fe catalysts showed superior selectivity compared to Ni for the reaction of furfural to methyl furan. Their theoretical calculations indicated that the oxophilic nature of Fe stabilizes the η^2(C,O) configuration of the aldehyde carbonyl, weakening the C—O bond and suppressing the formation of acyl intermediates that undergo decarbonylation [9]. High selectivities have also been reported for HDO reactions over Pd-Cu alloys [15]. In this example, the HDO selectivities improved from 20% for a Pd-only catalyst to 75% for the Pd-Cu alloy. Although Cu is not oxophilic, DFT calculations suggested that Cu atoms at the surface repel the aromatic furan ring [16], causing furfural to preferentially adsorb in an η^1(O)-aldehyde configuration via the carbonyl oxygen. Such an orientation of the furan ring prevents side reactions on the ring itself [9,15,16]. Finally, recent work by some of us on the Pt-Co system showed that Co tends to form a CoO_x shell on a Pt-rich core and that this oxide layer prevents interactions between the Pt and the furan ring, enhancing DMF yields from HDO of HMF [11].

In the present work, we examined the catalytic properties of other Pt alloys, including carbon-supported Pt-Ni, Pt-Zn, and Pt-Cu alloyed NCs prepared by solvothermal methods, in order to determine whether Pt-Co is unique among the Pt alloys in providing high selectivities for HDO of HMF. While Ni is catalytically similar to Co, Zn and Cu have properties that contrast sharply with that of Co and provide a test for the properties required for high selectivities (>95%). Surprisingly, each of the alloys exhibited superior selectivities compared to the monometallic catalysts. By using bimetallic, NCs catalysts with highly uniform compositions and monodispersities, we were also able to demonstrate that there are optimal compositions for the alloy catalysts.

2. Experimental

2.1. Catalyst synthesis

2.1.1. Chemicals

The following chemicals were used in the synthesis of the metal NCs: Nickel (II) acetate tetrahydrate ($Ni(ac)_2{\cdot}4H_2O$, Sigma-Aldrich, 98%), platinum (II) acetylacetonate ($Pt(acac)_2$, Acros, 98%), nickel (II) acetylacetonate ($Ni(acac)_2$, Acros Organics, 96%), copper (II) acetylacetonate ($Cu(acac)_2$, Sigma-Aldrich, ≥99.9%), zinc (II) acetylacetonate ($Zn(acac)_2$, Acros Organics, 25% Zn), 1,2-hexadecanediol (HDD, Sigma-Aldrich, 90%), tri-*n*-octylamine (TOA, Acros Organics, 97%), oleylamine (OLAM, Sigma-Aldrich, 70%), oleic acid (OLAC, Sigma-Aldrich, 90%), and trioctylphosphine (TOP, Sigma-Aldrich, 97%), borane, *tert*-butylamine complex, (BTB, Strem Chemicals, 97%), diphenyl ether (DPE, Sigma-Aldrich, 99%) and 1,2-dichlorobenzene (DCB, Acros Organics, 99%). Nickel(II) nitrate hexahydrate ($Ni(NO_3)_2{\cdot}6H_2O$, Alfa Aesar, 98%), Zinc(II) nitrate hexahydrate ($Zn(NO_3)_2{\cdot}6H_2O$, Alfa Aesar, 99%), Copper(II) nitrate trihydrate ($Cu(NO_3)_2{\cdot}3H_2O$, Alfa Aesar, 98%), and Cobalt(II) nitrate hexahydrate ($Co(NO_3)_2{\cdot}6H_2O$, Aldrich, 99%).

2.1.2. Synthesis of Pt_6Ni and PtNi NCs

The Pt_6Ni and PtNi NCs were synthesized using a scaled-up method reported previously [17]. For the Pt_6Ni NCs, $Ni(ac)_2{\cdot}4H_2O$ (0.33 mmol) and HDD (1.15 mmol) were dissolved in a solution of DPE (40 mL), OLAM (0.8 mL), and OLAC (0.8 mL). The reaction mixture was kept at 80 °C for 30 min under vacuum and then heated to 200 °C under a nitrogen atmosphere. $Pt(acac)_2$ (0.67 mmol), dissolved in DCB (2.4 mL), was injected into this mixture at 200 °C. The resulting solution was kept at 200 °C for 1 h before cooling to room temperature. The resulting NCs were then purified by precipitation with ethanol and centrifugation at 8000 rpm for 5 min. The precipitate was washed twice with hexane/ethanol (1:3) mixtures before the final NCs were dispersed in hexane. The same procedure was used to synthesize PtNi NCs, except that the amounts of $Ni(ac)_2{\cdot}4H_2O$ (2 mmol) and OLAC (1.0 mL) were adjusted. Also, after the washing steps, the PtNi NCs were re-dispersed in hexane and size-selective precipitation was performed [18].

2.1.3. Synthesis of Pt_3Ni NCs

To synthesize Pt_3Ni NCs, $Ni(acac)_2$ (0.4 mmol) and $Pt(acac)_2$ (0.4 mmol) were dissolved in a solution of TOA (40 mL), OLAM (5.44 mL), OLAC (1.28 mL), and TOP (0.45 mL). The reaction mixture was kept under vacuum at 70 °C for 30 min, then heated to 330 °C under a nitrogen atmosphere. After 30 min, the reaction mixture was cooled to room temperature and purified by precipitation with a mixture of isopropanol and ethanol. After being centrifuged at 8000 rpm for 2 min, the precipitate was washed twice with hexane/ethanol (1:3) mixtures. Finally, the NCs were dispersed in hexane.

2.1.4. Synthesis of PtCu and Pt_2Zn NCs

PtCu and Pt_2Zn NCs were synthesized by modifying a previously reported method [19]. For PtCu NCs, $Pt(acac)_2$ (0.4 mmol), $Cu(acac)_2$ (0.4 mmol), and BTB (1.1 mmol) were dissolved in OLAM (20 mL). The reaction mixture was kept under vacuum at 80 °C for 30 min before heating to 300 °C at a rate of 5 °C min^{-1}. After 1 h, the reaction mixture was cooled to room temperature. Purification of the NCs was achieved by addition of isopropanol, followed by centrifugation at 8000 rpm for 2 min. The precipitate was washed three times with hexane/ethanol (1:3) mixtures and the final NCs were dispersed in hexane. For Pt_2Zn NCs, $Pt(acac)_2$ (0.5 mmol), $Zn(acac)_2$ (0.5 mmol) and BTB (1.1 mmol) were dissolved in OLAM (20 mL). The reaction conditions and purification steps were the same as those for PtCu NCs synthesis.

2.1.5. NC characterization

The TEM images of NCs were collected on a JEOL JEM-1400 microscope operating at 120 kV and HRTEM on a JEOL JEM-2100 operating at 200 kV. Particle-size distributions were determined by small-angle X-ray scattering (SAXS) performed at Penn's Multi-Angle X-ray Scattering Facility and analyzed by Datasqueeze software [20]. Sample collection time was 1 h. The average sizes and size distributions were presented as (diameter) ± (standard deviation) nm. The elemental composition and concentration of NCs were determined by Inductively Coupled Plasma-Optical Emission spectrometry (ICP-OES) performed on a Spectro Genesis spectrometer with a concentric nebulizer. Powder X-ray diffraction (XRD) patterns were collected in the 2θ range between 20° and 80° on a Rigaku Smartlab high-resolution diffractometer with Cu Kα radiation (λ = 0.15416 nm).

2.1.6. Preparation of supported NCs

To prepare catalysts from the NCs, the NCs, dispersed in hexane, were mixed with carbon powder (Cabot, Vulcan XC72R) to a loading of 10-wt% metal. After sonication for 15 min, the solution was centrifuged at 6000 rpm for 1 min. The supernatant was removed and the precipitate was washed twice with isopropanol, followed by centrifugation. After drying each sample in a vacuum oven overnight at 50 °C, the samples were first treated with an O_2 plasma cleaner (18 W, Harrick Plasma) for 15 min, then transferred

for 1 min into a muffle furnace that had been preheated to 500 °C [21].

2.1.7. Synthesis of conventional Ni/C, Co/C, Cu/C, and Zn/C catalysts

The 10-wt% Ni/C, Co/C, Cu/C and Zn/C catalyst in this study were prepared by impregnation, using an identical procedure that is consistent with those in previous studies [8]. The Ni, Zn, Cu and Co precursors were $Ni(NO_3)_2{\cdot}6H_2O$, $Zn(NO_3)_2{\cdot}6H_2O$, $Cu(NO_3)_2{\cdot}3H_2O$, and $Co(NO_3)_2{\cdot}6H_2O$, respectively. Each metal precursor was firstly dissolved in a water/ethanol (5:1) solution and then mixed with carbon black (Vulcan XC-72R). After drying the catalyst at room temperature, the resulting powder was heated in flowing He to 500 °C for 6 h, using a heating ramp of 3 °C min^{-1}. The dried powders were reduced by flowing a 5% H_2/He mixture over the catalysts at 60 mL min^{-1} while ramping the temperature at 2 °C min^{-1}–400 °C, followed by heating to 500 °C with heating ramp of 1 °C min^{-1}. The catalysts were then held at this temperature for 2 h.

2.2. Reaction measurements

The liquid-phase HDO of HMF was performed in a continuous flow reactor which has been described elsewhere [8,22]. The reactor was a stainless-steel tube, 20 cm long and with a 4.6-mm ID. The typical catalyst loading was 0.05 g. For experiments requiring lower space times, the catalyst was diluted with additional carbon while keeping the total reactor loading at 0.05 g. The catalyst was packed in the middle portion of the tubular reactor and held by glass wool. To prevent the catalyst from being pushed from the center of the tube, an inert glass tube was placed downstream from the catalyst bed. The liquid feed, a mixture of 1.0 g HMF (99%, Sigma-Aldrich) and 100 mL of 1-propanol (Fisher Scientific), was introduced into the reactor using an HPLC pump (Series I+, Scientific Systems Inc.), which was also used to measure the total pressure in the reactor. The gas feed, H_2 (UHP grade, Airgas), was co-fed into the reactor through 0.002-inch ID capillary tubing (Valco Instruments, Inc.) and the gas flow rate was controlled by adjusting the pressure drop across the capillary tubing. A bubble meter at the reactor exit was used periodically to check the H_2 flow rates. The liquid flow rates could be varied from 0.02 to 0.2 mL min^{-1}, while the H_2 flow rates were 2–20 mL min^{-1} (STP). The ratio of the liquid and gas flow rates was kept constant in all experiments. A back-pressure regulator (KPB series, Swagelok) was placed at the reactor exit in order to control the pressure within the reactor.

Before carrying out reactions, the catalysts were pretreated at 250 °C in 1-bar, flowing H_2 for 30 min. The liquid products were collected and analysis was performed using syringe injection into a GC–MS (QP-5000, Shimadzu), equipped with a capillary column (HP-Innowax, Agilent Technologies). The gas-phase products were also examined but were found to consist of only H_2 and solvent vapor. Quantification of the major products was accomplished by calibration with standard solutions of HMF, DMF, DMTHF, 2-hexanone, 2-hexanol, and 2,5-hexandione (all purchased from Sigma Aldrich). The GC sensitivities for furanic-intermediate products were assumed to be the same as that for HMF, while the GC sensitivities for open-ring ether products were assumed to be the same as that of 2-hexanone. Based on repeated measurements, the uncertainty in the conversions and yields was less than 5% in all cases, and the carbon balances were above 95% in all cases. The measurement times for each experiment were approximately 4 h and most of the data used in this manuscript were taken 40–60 min after starting the reaction. For the conditions of this study, there was no reaction in the absence of a catalyst. The space times (W/F) in this work were given as the weight of the metal catalyst divided by the volumetric flow rates of the liquid.

3. Results

3.1. Nanocrystal catalyst characterization

Nearly monodisperse Pt-based alloyed NCs with various compositions were synthesized by solvothermal synthesis, which enabled us to investigate the composition dependent catalytic behavior of the bimetallic NCs. TEM images of the Pt_6Ni, Pt_3Ni and PtNi NCs are shown in Fig. 1a)–c) and indicate that, in each case, the particles are uniform and spherical in shape. Based on the small-angle X-ray scattering (SAXS) data fitted to Rayleigh function (Fig. 1d)), the average sizes and size distributions of the Pt_6Ni, Pt_3Ni, and PtNi NCs were 3.0 ± 0.4, 3.0 ± 0.6 and 6.0 ± 0.8 nm, respectively. As shown in Fig. 1e), the XRD patterns for each of the NCs showed a face-centered cubic (fcc) crystal structure, and shifts to higher angles in the peaks at 2θ were observed for Pt_6Ni and PtNi NCs, compared with the pure Pt NCs. This results from a contraction of the lattice based on the Vegard's law [23] and is a good indication that the NCs are well-mixed bimetallics. In the case of Pt_3Ni NCs, the only observed 2θ peak corresponds to the (111) plane. The absence of additional peaks suggests either polycrystallinity or the presence of a high concentration of defects, as is often seen with NC systems [24]. There was essentially no change in the morphology or size of the NCs following their addition to the carbon support and their treatment to remove the ligands by O_2 plasma and thermal annealing. This is demonstrated by the TEM images shown in Figs. S1a)–c).

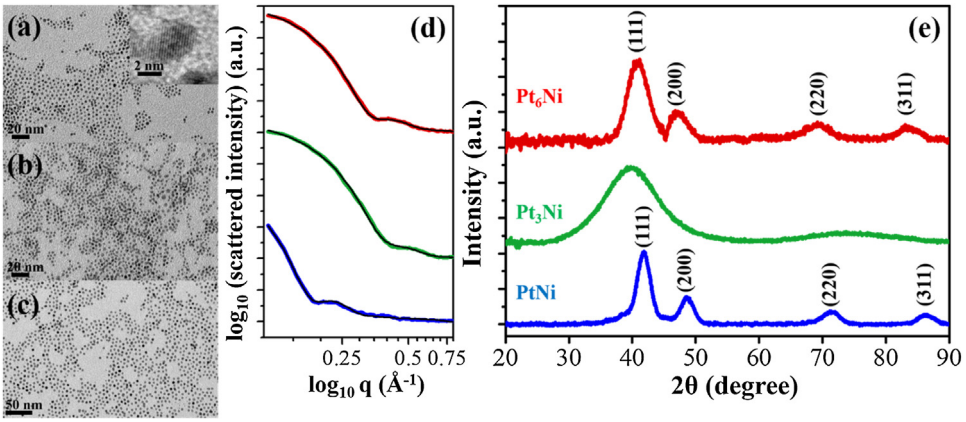

Fig. 1. The TEM images of (a) Pt_6Ni, (b) Pt_3Ni and (c) PtNi NCs, the corresponding (d) SAXS patterns and (e) XRD patterns. Inset in (a) shows the HRTEM image of Pt_6Ni NCs. The black lines in (d) represent the simulated fits for the size of the catalyst.

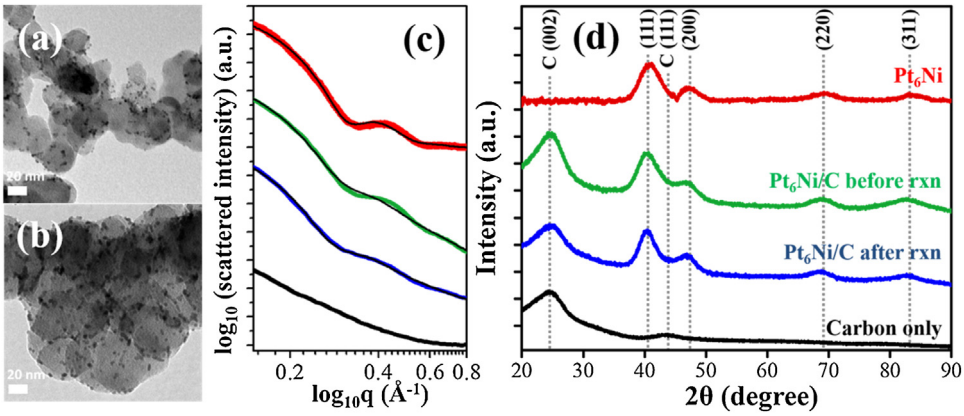

Fig. 2. The TEM images of 10-wt% Pt_6Ni NCs on carbon support (a) before and (b) after reaction. (c) SAXS patterns of Pt_6Ni NCs in solution (red), 10-wt% Pt_6Ni NCs on carbon support before (green) and after (blue) reaction, carbon support (black), and (d) the corresponding XRD patterns. The black lines in (c) represent the simulated fits for the size of the catalyst. (For interpretation of the references to colour in this figure legend, the reader is referred to the web version of this article.)

The Pt-Ni NC catalysts also exhibited good stability under HDO reaction conditions. Fig. 2 shows TEM images of the catalysts based on Pt_6Ni NCs before (Fig. 2a)) and after (Fig. 2b)) 5 h of HDO reaction. The thermal stability of NC catalysts was further confirmed by SAXS measurements (Fig. 2c)). By subtracting out the scattering from carbon support (black curve) and performing fitting with Rayleigh function, the average sizes of Pt_6Ni/C before (green curve) and after (blue curve) the functional testing were 4.1 ± 0.8 and 4.1 ± 0.7 nm, respectively. The results from SAXS measurements indicate no change in the size of the NCs consistently with TEM observations. The XRD patterns (Fig. 2d)) measured before (green curve) and after (blue curve) the catalyst was exposed to the reaction environment also indicated that there was no phase transformation from disordered fcc to ordered face-centered tetragonal (fct) structure. The carbon support was measured as a control (black curve) and peaks near 25° and 43° correspond to graphite (002) and diamond (111) planes for Vulcan carbon supports [25]. The thermal stability of crystal structure makes it possible to exclude a contribution from structural ordering on the catalytic performance.

Similar characterization studies were performed with the catalysts prepared from PtCu and Pt_2Zn NCs, with TEM images shown in Fig. 3a–b. The addition of a stronger reducing agent (BTB) resulted in smaller NCs than the ones prepared without BTB, which is consistent as reported [19]. XRD patterns of the as-synthesized PtCu and Pt_2Zn NCs also showed fcc structure (Fig. 3d)). Based on SAXS data fitted to Rayleigh function (Fig. 3c)), the average sizes and size distributions of the PtCu and Pt_2Zn NCs are 6.6 ± 1.2 and 2.6 ± 0.6 nm, respectively. The catalyst characterizations discussed above indicate that the NCs synthesized by solvothermal methods were excellent subjects to study the bimetallic catalyst composition dependent HDO of HMF.

3.2. Hydrodeoxygenation of HMF in a continuous flow reactor

In previous studies, we showed that the HDO reaction for HMF in several alcohol solvents is a series reaction, with products forming as shown in Scheme 1 [8,22]. The HMF (A) is first converted to a group of partially hydrogenated intermediate species (B), including 2-propoxymethyl-5-furanmethanol (ether-furfuryl alcohol, or EFA), 2-propoxymethyl-5-methylfuran (ether-methyl furan, or EMF), 5-methylfurfural (MF), 2-hydroxylmethyl-5-methylfuran (HMMF), 2,5-bis(hydroxymethyl)furan (BHMF), and 2,5-bis(propoxymethyl)furan (BEF). All these intermediates can react further to form DMF (C), which in turn reacts to over-hydrogenated products (D), such as DMTHF 2-hexanone, 2-hexanol, 2,5-hexanedione, and their etherification derivatives, 1-propoxy-1-methylpentane (2-propoxyhexane) and 1,4-dipropoxy-1,4-dimethylbutane (2,5-dipropoxyhexane). All of the studied monometallic catalysts, including carbon-supported Pt, Pd, Ir, Ru, Co, and Ni, were found to exhibit relatively poor selectivity for DMF

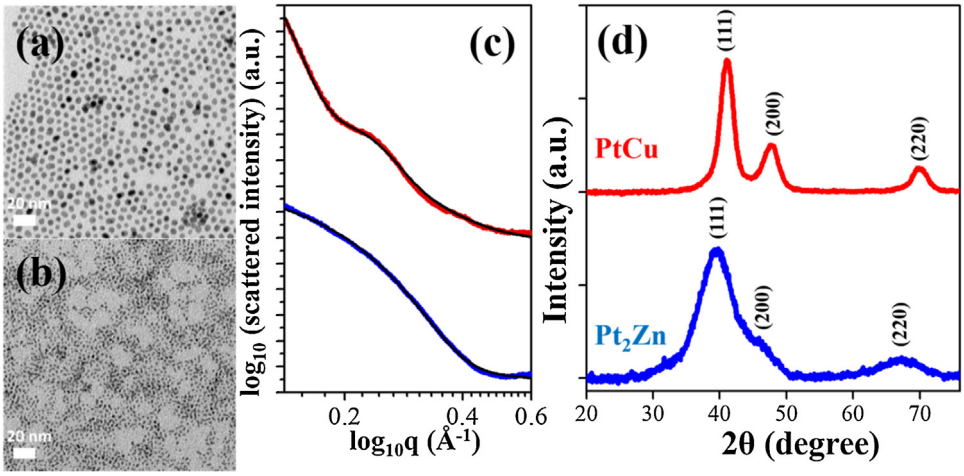

Fig. 3. The TEM images of (a) PtCu and (b) Pt_2Zn NCs, the corresponding (c) SAXS patterns and (d) XRD patterns. The black lines in (c) represent the simulated fits for the size of the catalyst.

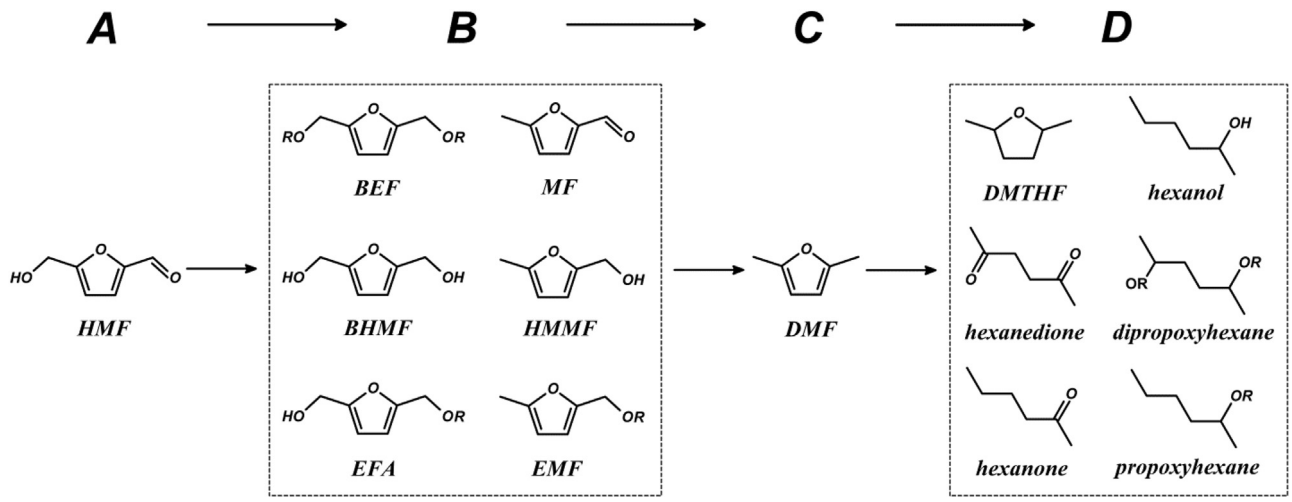

Scheme 1. Reaction network for HDO of HMF using alcohols as solvent.

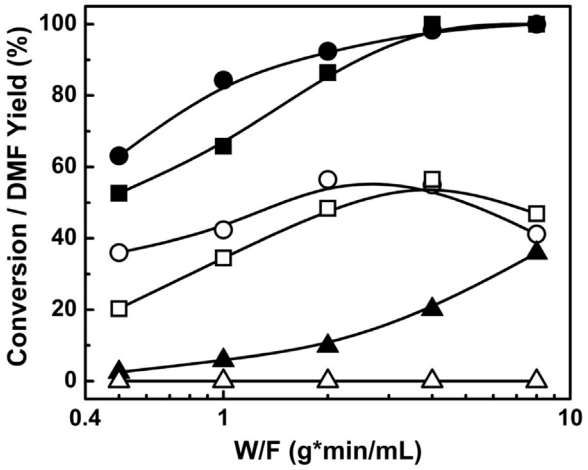

Fig. 4. Conversion and DMF yield for the HDO reaction of HMF over impregnated 10-wt% monometallic catalyst, as a function of reactor space time. Reaction conditions: 33 bar and 180 °C. (●) HMF conversion on Ni/C, (○) DMF yield on Ni/C, (■) HMF conversion on Co/C, (□) DMF yield on Co/C, (▲) HMF conversion on Cu/C, (△) DMF yield on Cu/C. Zn/C catalysts did not show any activity (not reported).

formation [8,11,22]. DMF yields varied with the particular metal catalyst and the reaction conditions but were typically less than about 50%. The products formed by the further reaction of DMF also varied with the metal catalyst, with Pt tending to form open-ring products, primarily 2-hexanone and 2-propoxyhexanone [8].

Fig. 4 shows a comparison of HMF conversions and DMF yields at 180 °C and 33 bar total pressure for conventional Ni/C, Co/C, and Cu/C catalysts with 10-wt% metal. Results for Ni/C and Co/C are similar to what was reported previously [8]. Both catalysts show high conversions, over 50%, for even short residence times; and the DMF yield goes through a maximum of slightly more than 50% with increasing space time, decreasing with longer space times. The detailed product distributions are reported elsewhere [8], but the major over-hydrogenated product for both metals was 2,5-hexandione. By contrast, the Cu/C was much less active, with a maximum conversion of less than 40% at the longest space time studied. The only products formed over the Cu/C catalyst were those in the B group of Scheme 1, including MF, HMMF and BEF, with yields listed in Table S1. The low HDO activity observed over Cu agrees with previous literature hydrogenation reactions of furfural over Cu catalysts, which shows that the reaction over Cu tends to stop with formation of furfuryl alcohol [15]. Zn/C catalysts did not show any activity for HDO of HMF under the conditions of this study.

The bimetallic catalyst, Pt-Co, can be highly selective for production of DMF, with 98% yield for optimized metal compositions and reaction conditions [11]. The high selectivity in that case was the result of DMF being unreactive, so that the sequential reaction stopped at DMF. Furthermore, because both Pt and Co are able to catalyze the reaction of DMF to over-hydrogenated products, exceptional selectivity was only observed when the bimetallic NCs were prepared by solvothermal synthesis. Bimetallic catalysts prepared by conventional infiltration of the metal salts were less selective due to non-uniformities in the local composition of the metal particles.

To determine how other bimetallic catalysts would perform in comparison to Pt-Co, similar experiments were performed over the Pt-Ni, Pt-Cu, and Pt-Zn bimetallic catalysts. Fig. 5 reports the HMF conversion and product yields as a function of space time for the three Pt-Ni/C catalyst at 160 °C and 33 bar. The results are qualitatively similar for all three Pt-Ni catalysts, although the Pt_3Ni/C catalyst in Fig. 5b) showed somewhat lower conversions. At a space time of 0.5 g min mL^{-1}, the conversion over Pt_3Ni/C was around 85%, while the conversions on the other two Pt-Ni catalysts were over 95%. In general, HMF conversion increased steadily with space time, while partially hydrogenated products (B group) yield diminished in favor of DMF formation. Except for Pt_3Ni/C, DMF yield reached a value of 80–90% before decreasing due to over-hydrogenated products (D group) formation. The fact that the D products form at the same space times for which DMF yields begin to decrease suggests that they are formed from DMF. The major D product observed with the Pt_6Ni/C catalyst was 2-hexanone, the same major product formed on Pt catalysts [8,22], while with PtNi/C 2,5-hexandione was observed, which was also the primary product formed on Ni/C catalysts [8]. Interestingly, no over-hydrogenated products were observed on the Pt_3Ni/C catalyst for even the highest space time examined. A more detailed analysis of the B and D compounds yield is given in the Supplemental Information, Table S2a.

Because the conversions for the Pt_3Ni/C were low at 160 °C, additional measurements were performed on this catalyst at 200 °C, with results reported in Fig. 6. At this temperature, the conversions of HMF were much higher. Furthermore, DMF yields reached 98% at the higher space times. It is not likely that the higher yields are due to the increase in temperature. In addition to the fact that previous work indicated that selectivities are not very different between 100 and 200 °C [11,22], one would expect the reaction

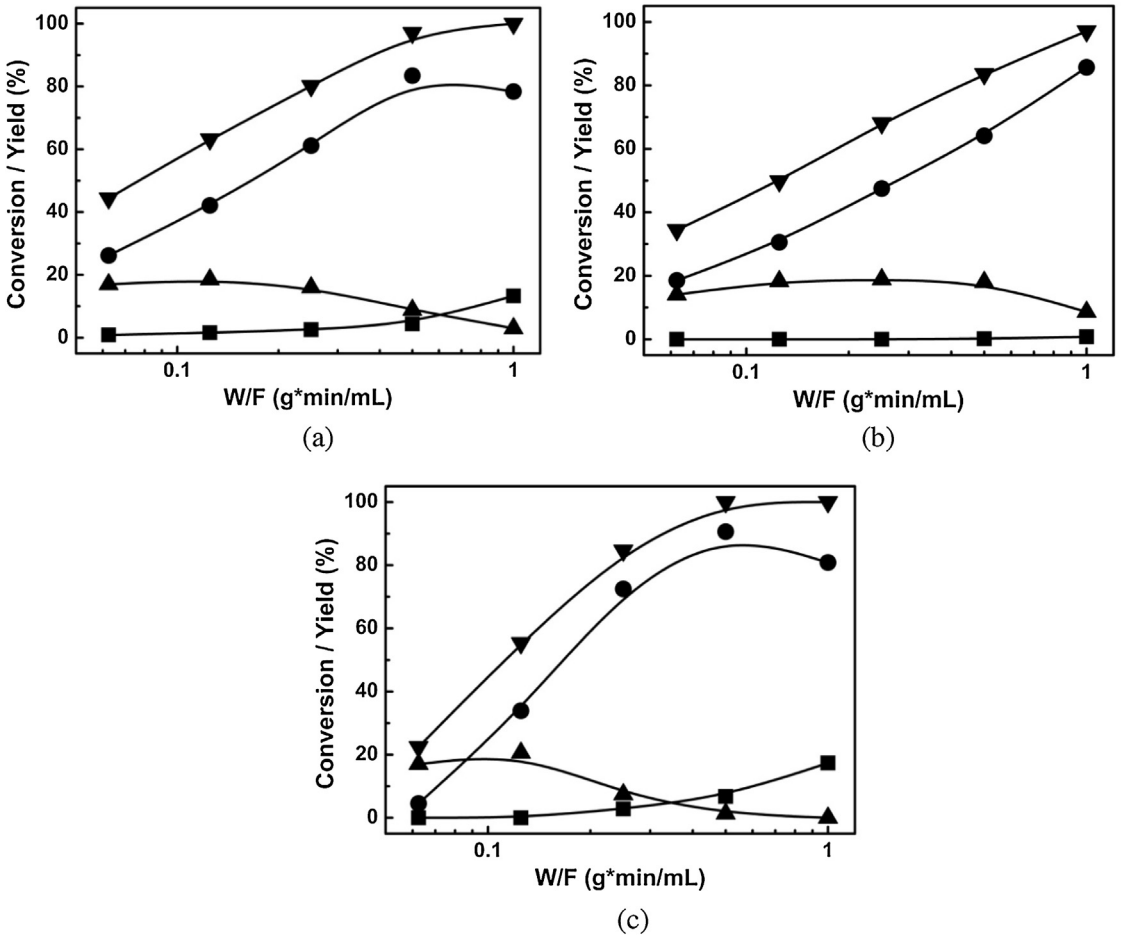

Fig. 5. Conversion and product distribution for the HDO reaction of HMF over (a) 10-wt% Pt_6Ni/C, (b) 10-wt% Pt_3Ni/C, (c) 10-wt% PtNi/C, as a function of reactor space time. Reaction conditions: 33 bar and 160 °C. (▼) HMF conversion, (▲) product group B, (●) DMF, (■) product group D.

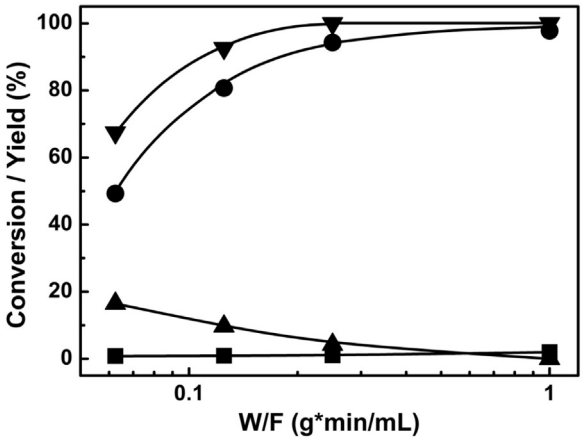

Fig. 6. Conversion and product distribution for the HDO reaction of HMF over 10-wt% Pt_3Ni/C, as a function of reactor space time. Reaction conditions: 33 bar and 200 °C. (▼) HMF conversion, (▲) product group B, (●) DMF, (■) product group D.

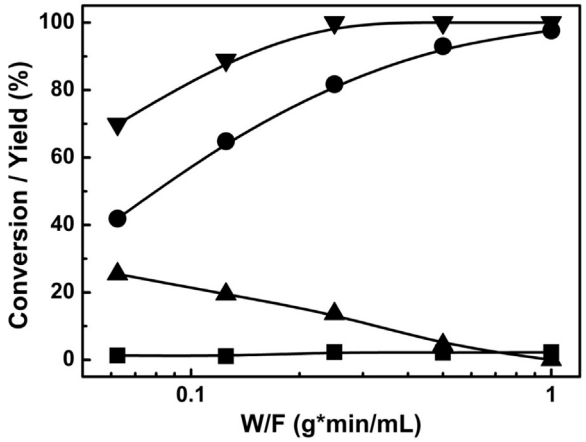

Fig. 7. Conversion and product distribution for the HDO reaction of HMF over 10-wt% Pt_2Zn/C, as a function of reactor space time. Reaction conditions: 33 bar and 200 °C. (▼) HMF conversion, (▲) product group B, (●) DMF, (■) product group D.

of DMF to over-hydrogenated products to increase with temperature. The maximum in the yield as a function of space time in Fig. 6 is clearly less steep than that found for Pt_6Ni/C and PtNi/C catalysts. Furthermore, the Pt_3Ni/C catalyst was remarkably stable. There was no observable change in either the conversion or the DMF yield over a period of at least 5 h on the Pt_3Ni/C catalyst, while significant changes in both were observed on Pt/C and Ni/C catalysts. The data in Figs. 5 and 6 therefore indicate that the Pt-Ni catalysts are more selective and stable than their monometallic counterparts and that there is an optimum Pt:Ni ratio.

Catalysts based on Pt-Zn and Pt-Cu bimetallic NCs were also investigated, with results shown in Figs. 7 and 8. Because these catalysts were also less active than Pt/C, reactions were carried out at 200 °C and 33 bar. The results for 10-wt% Pt_2Zn/C in Fig. 7 are very

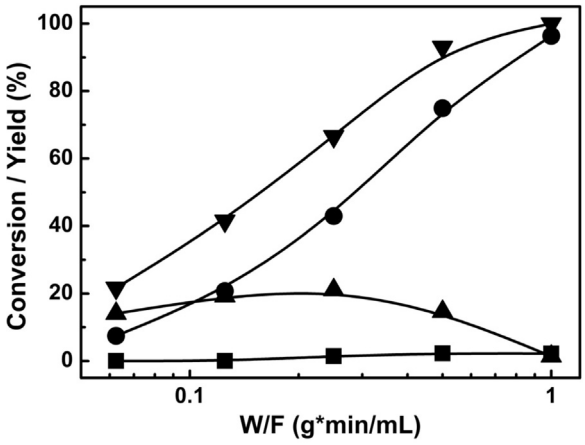

Fig. 8. Conversion and product distribution for the HDO reaction of HMF over 10-wt% PtCu/C, as a function of reactor space time. Reaction conditions: 33 bar and 200 °C. (▼) HMF conversion, (▲) product group B, (●) DMF, (■) product group D.

similar to results for Pt_3Ni/C, although the rates were slightly lower. Again, DMF yields as high as 98% were achieved at high space time, with negligible production of over-hydrogenated products. Similar performance was observed over the PtCu/C catalyst, Fig. 8, with DMF yields again reaching 96%. However, alloying the Pt with Cu did significantly decrease the rates.

4. Discussion

The results of the present study clearly demonstrate that the catalysts formed by alloying Pt with a number of metals can significantly increase the yields for the HDO reaction of HMF to DMF. In all cases, the increased yields result from a decreased reactivity of DMF to over-hydrogenated products. As pointed out in the Introduction, the alloying metals appear to do this in different ways but the net result in each case is that the alloying metal prevents the furan ring from lying down on the catalyst surface. With Pt-Co alloys, the furan ring is prevented from lying down on the surface by a "honey-comb", CoO_x overlayer on the Pt [11]. Since Ni is more easily reduced than Co, the effect of Ni on the bonding of the furans on the Pt-Ni alloys is likely due to the oxophilicity of the Ni, similar to what was reported for the effect of Fe on Ni-Fe alloy catalysts [9]. With Cu and Zn, the role of the alloying metals may be to change the Pt ensemble size or otherwise change the way the DMF bonds to the metal surfaces [13,15].

The selective alloy catalysts were also more stable. Previous work with monometallic catalysts based on Pt, Ni, and Co indicated that each showed significant deactivation over a period of three hours. Furthermore, deactivation appears to have been caused by coking, since the deactivation rates correlated with the carbon balances in the experiment. In the present study, there was no observable deactivation of a Pt_3Ni/C catalyst, consistent with what was also observed for a Pt_3Co_2 catalyst [11]. The likely explanation is that coking in this reaction is caused by the over-hydrogenated products. The over-hydrogenated products include di-ketones, which tend to be highly reactive.

With Pt-Ni and Pt-Co alloys, compositional uniformity of the catalyst is critical. Monometallic catalysts based on Pt, Ni, and Co are not selective because all three metals will catalyze the reaction of DMF to over-hydrogenated products [8]. Furthermore, the selectivity of the Pt-Ni and Pt-Co bimetallic catalysts depends on the Pt:Co [11] and Pt:Ni ratios. Synthesis of bimetallic catalysts by conventional methods in which the support is infiltrated with metal salts is not able to produce this uniformity, which is the reason we prepared the catalysts in this study by synthesizing uniform NCs in solution. With Pt alloys of Cu and Zn, the uniformity will be less important, given that Cu and Zn are not active for the reaction of DMF. In this sense, alloy catalysts based on Cu and Zn could be easier to synthesize.

The fact that various Pt alloys show good selectivities raises a number of interesting questions. First, would other alloys, including ones that do not include noble metals, also show high selectivity? Second, can one generalize the high HDO selectivity for HMF that is observed with the Pt alloys to HDO reactions with other reactants, such as those one might associate with lignin? These will be interesting questions to address in the future.

5. Conclusion

Carbon-supported, monometallic Pt and Ni catalysts exhibit relatively low selectivity, less than 50%, for DMF in the HDO reaction of HMF because DMF is converted to ring-opened or ring-hydrogenated byproducts. On the other hand, Zn and Cu catalysts are not active for HDO reactions. However, catalysts based on bimetallic Pt alloys with Ni, Zn, or Cu show significantly higher selectivity to DMF, up to 98%. With Pt-Ni alloys, controlling the local composition is critically important for achieving high DMF yields due to the non-selectivity of the pure metals. Even though the effects of Ni, Zn, and Cu on Pt are expected to be very different, it is likely that each of the alloys modifies the bonding of DMF so as to prevent the furan ring from lying down on the surface. This appears to be the critical factor in achieving high selectivity for HDO of HMF.

Acknowledgement

We acknowledge support from the Catalysis Center for Energy Innovation, an Energy Frontier Research Center funded by the U.S. Department of Energy, Office of Science, Office of Basic Energy Sciences under Award no. DE-SC0001004.

Appendix A. Supplementary data

Supplementary data associated with this article can be found, in the online version, at http://dx.doi.org/10.1016/j.apcatb.2016.06.051.

References

[1] T. Wang, M.W. Nolte, B.H. Shanks, Green Chem. 16 (2014) 548–572.
[2] M. Dashtban, A. Gilbert, P. Fatehi, RSC Adv. 4 (2014) 2037–2050.
[3] A.I. Torres, P. Daoutidis, M. Tsapatsis, Energy Environ. Sci. 3 (2010) 1560–1572.
[4] C.L. Williams, C.-C. Chang, P. Do, N. Nikbin, S. Caratzoulas, D.G. Vlachos, R.F. Lobo, W. Fan, P.J. Dauenhauer, ACS Catal. 2 (2012) 935–939.
[5] M. Chidambaram, A.T. Bell, Green Chem. 12 (2010) 1253–1262.
[6] T. Thananatthanachon, T.B. Rauchfuss, Angew. Chem. Int. Ed. 49 (2010) 6616–6618.
[7] J. Jae, W. Zheng, R.F. Lobo, D.G. Vlachos, ChemSusChem 6 (2013) 1158–1162.
[8] J. Luo, L. Arroyo-Ramírez, J. Wei, H. Yun, C.B. Murray, R.J. Gorte, Appl. Catal. Gen. 508 (2015) 86–93.
[9] S. Sitthisa, W. An, D.E. Resasco, J. Catal. 284 (2011) 90–101.
[10] G.-H. Wang, J. Hilgert, F.H. Richter, F. Wang, H.-J. Bongard, B. Spliethoff, C. Weidenthaler, F. Schüth, Nat. Mater. 13 (2014) 293–300.
[11] J. Luo, H. Yun, A. Mironenko, K. Goulas, M. Monai, J.D. Lee, C. Wang, P. Fornasiero, D.G. Vlachos, C.B. Murray, R.J. Gorte, ACS Catal. 6 (2016) 4095–4104.
[12] J.R. McManus, E. Martono, J.M. Vohs, ACS Catal. 3 (2013) 1739–1750.
[13] D. Shi, J.M. Vohs, ACS Catal. 5 (2015) 2177–2183.
[14] W. Yu, K. Xiong, N. Ji, M.D. Porosoff, J.G. Chen, J. Catal. 317 (2014) 253–262.
[15] S. Sitthisa, T. Pham, T. Prasomsri, T. Sooknoi, R.G. Mallinson, D.E. Resasco, J. Catal. 280 (2011) 17–27.
[16] S. Sitthisa, T. Sooknoi, Y. Ma, P.B. Balbuena, D.E. Resasco, J. Catal. 277 (2011) 1–13.
[17] K. Ahrenstorf, O. Albrecht, H. Heller, A. Kornowski, D. Görlitz, H. Weller, Small 3 (2007) 271–274.
[18] C.B. Murray, S. Sun, H. Doyle, T. Betley, MRS Bull. 26 (2001) 985–991.

[19] Y. Yu, W. Yang, X. Sun, W. Zhu, X.-Z. Li, D.J. Sellmyer, S. Sun, Nano Lett. 14 (2014) 2778–2782.
[20] Paul A. Heiney, Comm. Powder Diffr. Newsl. 32 (2005) 9–11.
[21] M. Cargnello, C. Chen, B.T. Diroll, V.V.T. Doan-Nguyen, R.J. Gorte, C.B. Murray, J. Am. Chem. Soc. 137 (2015) 6906–6911.
[22] J. Luo, L. Arroyo-Ramírez, R.J. Gorte, D. Tzoulaki, D.G. Vlachos, AIChE J. 61 (2015) 590–597.
[23] A.R. Denton, N.W. Ashcroft, Phys. Rev. A 43 (1991) 3161–3164.
[24] Y. Kang, X. Ye, C.B. Murray, Angew. Chem. Int. Ed. 49 (2010) 6156–6159.
[25] Y. Holade, C. Morais, K. Servat, T.W. Napporn, K.B. Kokoh, Phys. Chem. Chem. Phys. 16 (2014) 25609–25620.